

**VICTORIA UNIVERSITY**  
MELBOURNE AUSTRALIA

*Aluminum fumarate MOF/PVDF hollow fiber membrane for enhancement of water flux and thermal efficiency in direct contact membrane distillation*

This is the Accepted version of the following publication

Cheng, D, Zhao, L, Li, N, Smith, SJD, Wu, D, Zhang, Jianhua, Ng, D, Wu, C, Martinez, MR, Batten, MP and Xie, Z (2019) Aluminum fumarate MOF/PVDF hollow fiber membrane for enhancement of water flux and thermal efficiency in direct contact membrane distillation. *Journal of Membrane Science*, 588. ISSN 0376-7388

The publisher's official version can be found at  
<https://www.sciencedirect.com/science/article/pii/S0376738818335956>  
Note that access to this version may require subscription.

Downloaded from VU Research Repository <https://vuir.vu.edu.au/39166/>

**Aluminum fumarate MOF/PVDF hollow fiber membrane for  
enhancement of water flux and thermal efficiency in direct contact  
membrane distillation**

**Dongjian Cheng <sup>1,2</sup>, Lihua Zhao <sup>2,4</sup>, Na Li <sup>1,\*</sup>, Stefan J.D. Smith <sup>2</sup>, Dongyun Wu <sup>1</sup>,  
Jianhua Zhang <sup>3</sup>, Derrick Ng <sup>2</sup>, Chunrui Wu <sup>4</sup>, Marta Rubio Martinez <sup>2</sup>, Michael  
P. Batten <sup>2</sup>, Zongli Xie <sup>2,\*</sup>**

<sup>1</sup> Shaanxi Key Laboratory of Energy Chemical Process Intensification, School of Chemical Engineering and  
Technology, Xi'an Jiaotong University, Xi'an, Shaanxi 710049, P.R China

<sup>2</sup> CSIRO Manufacturing, Private bag 10, Clayton South MDC, VIC 3169, Australia

<sup>3</sup> Institute for Sustainability and Innovation, Victoria University, PO Box 14428, Melbourne, VIC 8001, Australia

<sup>4</sup> Institute of Biological and Chemical Engineering, Tianjin Polytechnic University, Tianjin 300387, PR China

---

\* Corresponding author. E-mail address: [lina@mail.xjtu.edu.cn](mailto:lina@mail.xjtu.edu.cn) (N. Li)  
[zongli.xie@csiro.au](mailto:zongli.xie@csiro.au) (Z. Xie)

## Abstract

Mixed matrix membranes combining the processibility of polymers with the properties of porous nano-additives is an effective method to enhance the performance of membrane distillation (MD) process. In this work, a new type of hydrophobic hybrid PVDF hollow fiber membranes doped with aluminum fumarate metal-organic frameworks (AlFu MOF) was fabricated and their performance in direct contact membrane distillation were studied experimentally and theoretically. The results showed that the addition of MOF particles efficiently enlarged the effective porosity of membrane and increased the water flux as well as the thermal efficiency of MD process. At 1 wt% MOF loading, the effective porosity of membrane was enlarged by 52.4%, which induced 55.9% increment in overall mass transfer coefficient of the hybrid membrane, and the thermal conductivity of the membrane was decreased by 38.6%, which contributed to the reduction of sensible heat loss of MD. Correspondingly, the experimental water flux of the hybrid 1 wt% MOF/PVDF membrane was improved by 50.5% and the thermal efficiency increased by 46.2% (0.58 vs 0.31) at a feed temperature of 40°C. Moreover, the MOF/PVDF membrane exhibited stable flux and retained high salt rejection (> 99.9%) for 3.5 wt% NaCl solution over a 50 h desalination test period. Overall, this study provides an insight into the positive effects of AlFu MOF additives on the enhancement of membrane performance in distillation process.

**Keywords:** MOF; hybrid PVDF hollow fiber membrane; water flux; thermal efficiency; direct contact membrane distillation.

## 1. Introduction

Water scarcity has caused considerable concerns on the sustainability of water resources due to the rapid and continuous industrialization, urbanization, and population growth [1,2]. Membrane distillation (MD) can be applied in desalination and industrial wastewaters treatment consuming low grade heat for thermal driving [3]. The alternative energy can be utilized such as geothermal energy, solar energy and waste grade heat from industrial streams. Generally, porous hydrophobic membranes (or layers on composite membranes) are the key part of the process that only allow for vapor molecules transport under a driving force of vapor pressure difference whilst retain the non-volatile on retentate side. It can concentrate the solutions to the saturation point with a relatively stable flux. And the nonvolatile contaminants rejection is theoretically 100% [1,4–6]. On account of these benefits, MD could be used as supplementary technique to reverse osmosis (RO) processes [2].

The primary influencing aspects hindering the MD's widely application are low water flux, high energy consumption, complex transport processes (in comparison to RO), and membrane wetting & fouling in long-term application [7]. In MD, the hydrophobic microporous membranes are mostly made from polyvinylidene fluoride (PVDF), polytetrafluoroethylene (PTFE), or polypropylene (PP) [1]. In principle, MD performance is determined by the membrane pore structure parameters including membrane thickness, average pore size, pore distribution, surface porosity, and geometry [2]. The polymeric membrane with higher porosity is favorable to achieve higher permeate flux and thermal efficiency in MD [8–12]. For example, Al-Obaidani et al. [9] reported that water flux and thermal efficiency of polypropylene membranes increased by 26% and 13% respectively due to 15% of increase in membrane porosity using four different membrane modules. As for membrane pore size, it should be large enough to obtain high flux on the premise of the non-wetting membrane pores. Recent research shows that the incorporation of appropriate nano-additives into the membrane could enhance MD performance on account of increased pore sizes and porosity, intensified surface roughness, and mechanical stability of membrane [13,14]. Yang et al. [15] claimed that the PVDF/MOF (iron 1,3,5- benzenetricarboxylate) membrane displayed a much higher water flux than the pristine PVDF membrane due to enlarged pore size and porosity. Yang et al. [16] found that the hybrid membranes blending with GO, HKUST-1 MOF, and HKUST-1@GO had wider pore channels on the supporting layers than the pristine cellulose

1 acetate membrane induced by the accelerated exchange between the solvent and non-solvent in the  
2 phase inversion process. Baghbanzadeh et al. [17] reported that the incorporation of the hydrophilic  
3 silica nanoparticles increased both surface porosity and average pore size of the PVDF membranes,  
4 which is beneficial for the enhancement of the permeate flux in VMD process. They believed that  
5 the nanoparticles acted as additional nucleating agents had the chance to infiltrate the polymer lean  
6 phase with the increase of the nano-additives concentration and help with the formation of larger  
7 surface porosity and pore size.

8 Among the nano-additives, metal-organic frameworks (MOFs) are hybrid materials consisting  
9 of inorganic metal centers or clusters connected by organic linkers to form flexible frameworks of  
10 various dimensional porous structures [18]. MOFs normally have large surface area and porosity,  
11 fine-tunable pore surface properties, low densities ( $0.2\text{--}1\text{ g/cm}^3$ ), and reasonable thermal and  
12 chemical stabilities [19,20]. They have been used as fillers in mixed matrix membranes for water  
13 treatment, pervaporation, and organic solvent nanofiltration to improve the liquid separation  
14 efficiency [21,22]. It is also known that many types of MOFs could lose structural integrity in an  
15 aqueous medium, which hinders their use in potential applications such as adsorption cooling and  
16 water desalination [15,23,24]. However, the MOFs with iron, zirconium, and aluminum metal ion  
17 clusters show reasonable stability in water applications [15,25]. Recently, MOF (iron 1,3,5-  
18 benzenetricarboxylate)/PVDF hybrid membranes prepared by electrospinning method were used in  
19 direct contact MD (DCMD) process and showed stable permeability and salt rejection [15]. In  
20 addition, a hydrophobic membrane with MOF-functionalized alumina surfaces was synthesized for  
21 saline water desalination in a vacuum membrane distillation (VMD) process and achieved a good  
22 wetting resistance with a high liquid entry pressure [25].

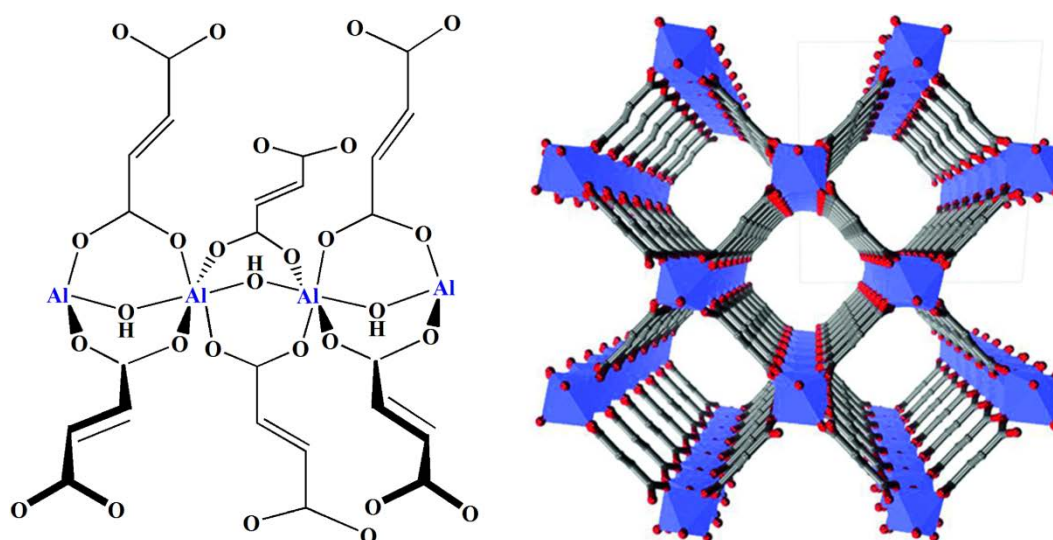


**Fig. 1.** Building block for aluminum fumarate metal organic framework (AlFu MOF) and section of the packing diagram (Al octahedra blue, O red, C gray. Hydrogen atoms have been omitted for clarity) [26]. (The copyright of this figure has been authorized by “John Wiley and Sons”)

Among various MOFs, aluminum fumarate MOF (AlFu MOF), which is commercially available [26], can be a good option for water treatment because of these benefits: 1) low production cost together with the use of a naturally occurring linker and a large amount of metallic cation; 2) exceptional water stability; 3) a permanently porous 3D structure; 4) and a scale-able and environmentally friendly synthesis from water and simple aluminum salts; with a huge production of up to 3600 kg/(m<sup>3</sup>·day) [26–30]. Therefore, the incorporation of AlFu MOF (shown in Fig. 1) is a promising and readily scalable option for high performance membrane for seawater desalination and wastewater treatment. To the best of our knowledge, hybrid MOF/PVDF hollow fiber membranes using AlFu MOF as additives in MD process for water application has not yet been investigated.

In this work, novel hydrophobic hybrid MOF/PVDF hollow fiber membranes with AlFu MOF as additives were prepared and their performance were evaluated in DCMD for desalination. The effects of the MOF dosages in the hybrid membranes on physical and chemical properties of membrane and DCMD performance were investigated. The theoretical models on mass and heat transfer of the hybrid membranes were built to correlate the permeate flux and thermal efficiency with membrane pore structure parameters to reveal the effect mechanism of MOF dosage on membrane performance. Finally, the membranes were subjected to 3.5 wt% NaCl aqueous solutions as feed for long-term stability test.

## 2. Materials and methods

### 2.1. Materials

PVDF powder (SOLEF 6010, France) was purchased from Solvay Solexis Company. Sodium chloride (NaCl, 99.5%) was purchased from Merck Millipore. The reagents were used as received. Dimethyl acetamide (DMAc, >99.9%, USA) was used as the solvent to prepare the PVDF dope solution. 1,2- propylene glycol (PG, Sigma-aldrich) was used as the non-solvent additive. The aluminum fumarate MOF (AlFu MOF) was provided by Rubio-Martinez and co-workers, who synthesized the AlFu MOF using a continuous flow reactor [29]. Briefly, streams of aqueous aluminum sulfate and sodium fumarate reacted in continuous flow conditions (65°C, residence time ca. 1 min). The product MOF was then washed sequentially with water and ethanol before vacuum drying at 80°C.

### 2.2. Synthesis of membranes

The MOF/PVDF hybrid hollow fiber membranes were fabricated using a dry-jet wet phase inversion method. To prepare the dope solutions, a certain amount of MOF particles (0, 0.5, 1, 2, 3, 4, and 5 wt% relative to the PVDF mass) were dispersed in DMAc (61.5 wt%) using DT 102H Bandelin ultrasonicator (Germany). Afterwards, PVDF powder (16.5 wt%) and PG (22.0 wt%) were added into MOF/DMAc solutions and mechanically stirred at 70°C to obtain homogenous dope solutions. Then, the stirring was stopped and the polymer solutions were kept at 70°C for 6 h to remove air bubbles. Hollow fiber membranes were fabricated through the spinning equipment as presented in Fig. 2. The polymer dope solution at 60°C was fed to the spinneret via a pump. DI water was pumped into the spinneret inner tube as bore liquid simultaneously to form the hollow fiber lumen side. The spinneret inner/outer diameters were 0.7 mm and 1.1 mm, respectively. The effluent dope solution from the spinneret passed through a 4 cm air gap and then immersed into a water coagulation bath at 70°C to form the hollow fiber membranes. These membranes were rinsed with fresh water to remove the residual solvent. At last, the membranes were dried in air at 25 °C to obtain the hydrophobic membranes.

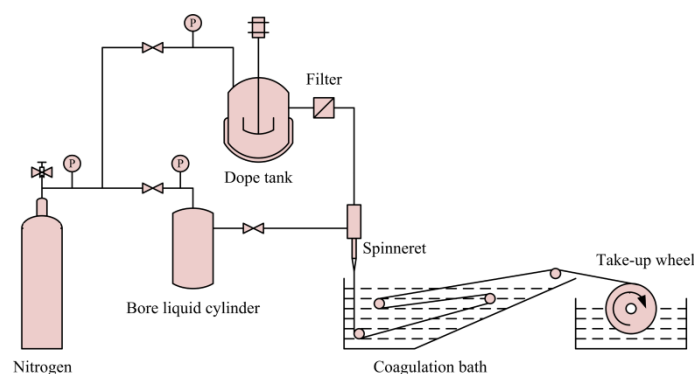


**Fig. 2.** Schematic of hollow fiber spinning apparatus.

### 2.3. MOF and membrane characterization

BET surface areas of the MOF particles were characterized using a Quantachrome Autosorb ASAP 2420 from N<sub>2</sub> adsorption isotherms at liquid nitrogen temperature (77 K). The size of MOF particles was characterized by a Saturn II Laser Diffraction Particle Sizer.

The presence of MOF in the MOF/PVDF membranes was detected by Fourier transform infrared spectrometer (FTIR, Thermo Scientific Nicolet 6700) equipped with an attenuated total reflection accessory including a ZnSe plate (45° angle of incidence). The FTIR spectra were recorded in a scanning range of 600–4000 cm<sup>-1</sup>.

Morphology of the prepared MOF/PVDF membranes was examined by a scanning electron microscope (SEM, Merlin ZIESS GEMINI2). The SEM image was carried out with working distance of 3.3-4.5 mm and voltage of 5 kV. Energy Dispersive X-ray Spectroscopy (EDS) was employed to test the elemental composition of the MOF nanoparticles and to observe the presence and dispersion of MOF nanoparticles in the hybrid membranes. SEM and EDS characterization of the samples were conducted after being covered in gold.

Thermal stabilities were investigated by Thermogravimetric (TGA) analysis under nitrogen conditions at a heating rate of 10 °C/min (from 0 to 800°C) using Perkin Elmer STA 6000. DSC was undertaken with a Mettler Toledo Differential Scanning Calorimeter with a temperature range of 25°C to 200°C and heating rate of 10°C/min. XRD patterns were recorded at 40 kV and 30 mA by a SHIMADZU XRD-6100 with a Cu cathode. 2θ range of 6–60° was performed with a scanning rate of 10 °/min.

The MOF/PVDF membranes' water contact angles (WCA) were tested by a KSV contact angle meter (CAM200). The measurement was conducted at room temperature by the sessile drop method,



equipped with an optical system to capture the profile of the tested liquids. The WCA of each membrane was the average value of measurement results at three different positions.

## 2.4. Gas permeation test

The mean pore size and effective porosity of the prepared membranes were measured by the gas permeation test [31,32]. The gas permeation flux via an asymmetric membrane is dependent on the combination of Poiseuille flow and Knudsen flow [33-35]. The mean pore size, porosity and effective porosity of the membranes can be obtained via Eqs. (S1-S3).

The experimental setup of gas permeation test is shown in Fig. 3. The membrane modules contained 3 hollow fiber membranes with 21 cm effective length and 1.5 cm inner diameter. In the test, the pure nitrogen permeated through the fibers under a trans-membrane pressure within 0.02–0.1 MPa at a pressure increment interval of 20 kPa and room temperature. The total gas permeation rate was observed by a wet flowmeter. The tests were repeated at least three times.

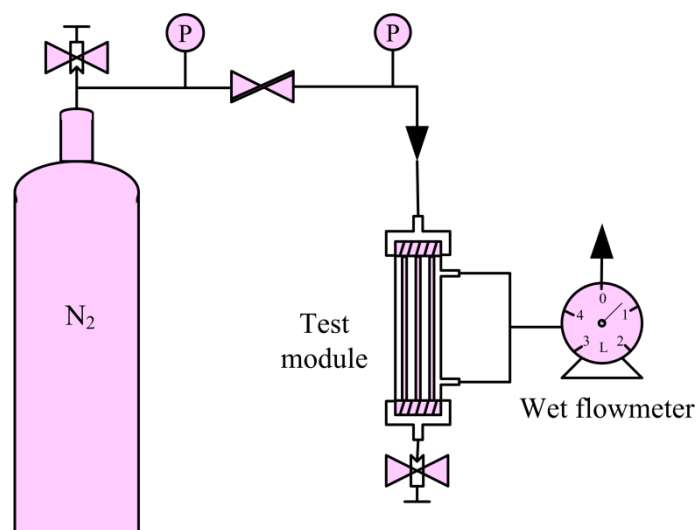


**Fig. 3.** Experimental setup for gas permeation test on membrane.

## 2.5. Membrane performance in DCMD process

The performances of the MOF/PVDF hollow fiber membranes with various MOF dosages (Fig. S1) were evaluated in DCMD experiment and the schematic diagram is presented in Fig. 4. The effective membrane area is 0.025 m<sup>2</sup>. All of the hybrid membranes' liquid entry pressure is higher than 200 kPa, which is high enough to prevent the membrane pore wetting in DCMD process. To ensure experimental reproducibility, 2 L of 1 wt% NaCl solution as the initial feed and 1 L of deionized water (< 5 μS/cm) as the initial distillate were used for each experiment. The feed was

circulated through the hollow fibers' lumen side and the deionized water was circulated through the membrane modules' shell side by peristaltic pumps. The feed temperature was adjusted and maintained by a heater and the permeate temperature was set at 20°C by a chiller. The inlet and outlet temperatures of the membrane module on feed/permeate side were measured by K-type thermocouples with  $\pm 1^\circ\text{C}$  accuracy. Both feed and permeate flow rates were monitored using rotor flow meters. The permeate stream was measured by weight gain using an analytical balance. The water flux,  $J$  ( $\text{kg}/(\text{m}^2\cdot\text{h})$ ), was calculated by:

$$J = \frac{\Delta W}{At} \quad (1)$$

where  $\Delta W$  (kg) denotes the mass increment of permeate over a given time  $t$  (h), and  $A$  ( $\text{m}^2$ ) is the effective membrane area.

The salt rejection was determined based on the measurement of the permeate conductivity using a digital conductivity meter. The salt rejection,  $\alpha$ , was calculated using the following expression:

$$\alpha = \left( 1 - \frac{c_p}{c_f} \right) \times 100\% \quad (2)$$

where  $c_f$  and  $c_p$  refer to the salt concentration in the bulk feed and in the permeate solutions, respectively.

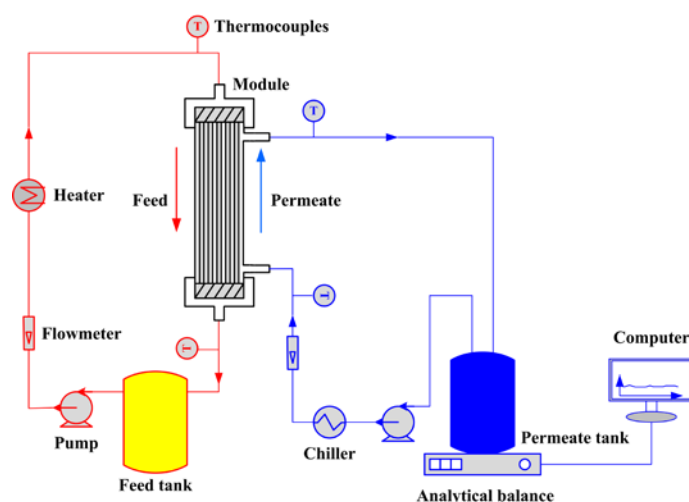


**Fig. 4.** Experimental DCMD setup used for desalination.

A summary of the vital theoretical equations of heat and mass transfer in DCMD is presented in Supporting Information. The membrane thermal conductivity ( $k_m$ ) can be obtained by Eq. (S18) where  $k_{p-m}$ ,  $k_g$ , and  $\varepsilon$  are the membrane material's thermal conductivity, the water vapors' thermal

conductivity, and the membrane surface porosity, respectively. The thermal conductivity of AlFu MOF ( $k_{mof}$ ) is assumed to be 0.12 W/(m·K) [33] and the MOF percentage in MOF/PVDF mixed materials ( $\omega$ ) is considered for calculating the thermal conductivity of the materials. Consequently, combining Eq. (S13-S17), the parameters of  $T_{mf}$ ,  $T_{mp}$ , and  $J$  can be determined, and then the thermal efficiency can be acquired as below [3,34]:

$$\eta = \frac{J\Delta H_v}{J\Delta H_v + \frac{k_m}{\delta_m}(T_{mf} - T_{mp})} \times 100 \quad (3)$$

### 3. Results and discussion

#### 3.1. MOF and MOF/PVDF hybrid membrane characterizations

##### 3.1.1. AlFu MOF characterizations

The characterized morphology and elemental composition of AlFu MOF particles and their dispersion in membrane are presented in Fig. 5. The size of the AlFu MOF crystals is about 100-200 nm and agglomerate together into large particles (Fig. 5 (a)). Fig. 5 (b) confirmed the presence of the characteristic Al element of the AlFu MOF particles. From Fig. 5(c), it can be seen that the size of MOF particles distribute in a range of 100-200 nm. Fig. 5(d) shows that the average pore diameter of MOF (0.6 nm) is larger than the diameter of water vapor molecules (0.28 nm diameter) and thus should allow fast permeation through the pore channels when incorporated into a DCMD membrane. Moreover, the specific surface area of the MOF is around 1000-1100 m<sup>2</sup>/g and the total pore volume is about 0.7473 cm<sup>3</sup>/g by the BET test.

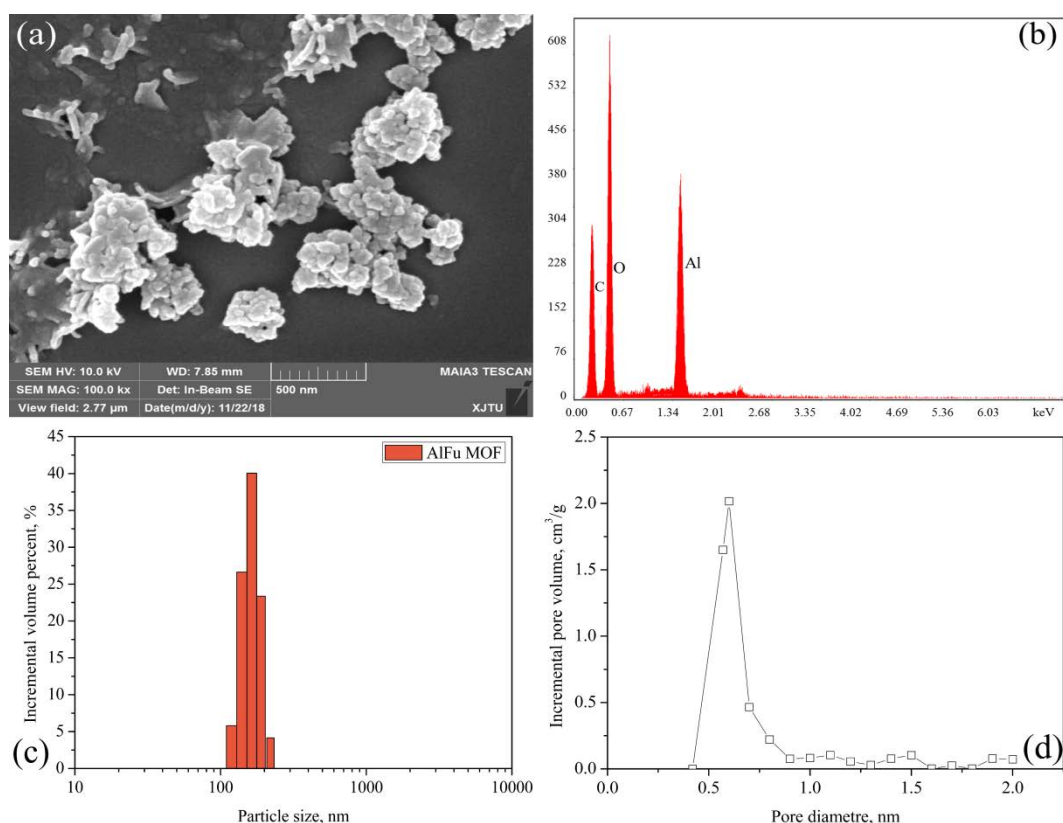


Fig. 5. (a) SEM image, (b) EDS, (c) particle size distribution, and (d) pore diameter of the AlFu MOF

nanoparticles.

### 3.1.2. FTIR, TGA, DSC, and XRD analysis of membranes

Fig. 6 (a) illustrates the Fourier transform infrared (FT-IR) spectra of the AlFu MOF, original PVDF, and the hybrid MOF/PVDF membranes. As for the AlFu MOF, the peaks of  $560\text{ cm}^{-1}$ ,  $930\text{ cm}^{-1}$ , and  $1625\text{ cm}^{-1}$  related to the Al-OH bond, the O-H bond, and the C=C bond, respectively. Comparing to the pristine PVDF membrane, a new absorption peak appears at  $1625\text{ cm}^{-1}$  for MOF/PVDF membranes. The peak is attributed to C=C bonds present in the MOF's fumarate linker groups, confirming the inclusion of the AlFu MOF in the prepared hybrid MOF/PVDF hollow fiber membranes.

The MD membrane should be thermally stable and the TGA analysis was performed to study the influence of MOF dosage on the thermal properties of the MOF/PVDF membranes. As presented in Fig. 6 (b) and Table 1, the main weight loss for MOF and PVDF occurs from 460 to 480  $^{\circ}\text{C}$  while the decomposition occurs at lower temperature for the MOF/PVDF membranes and that degradation temperature ( $T_d$ ) decreases with the increasing of MOF loading. This means that the addition of MOF particles and the resulting interaction between MOF and PVDF catalyzes the thermal

1 degradation of the PVDF membrane. However, the degradation temperature for the up to 5%  
2 addition of MOF in PVDF membrane (360-390°C) is still much higher than the operation  
3 temperature range in DCMD process (30-80°C), meaning that the reduced thermal stability of the  
4 prepared hybrid membranes does not impact its application in the membrane distillation process.

5 The effect of the addition of MOF on the crystallinity of MOF/PVDF membranes was  
6 investigated through DSC analysis. As shown in Fig. 6 (c), the nucleation temperature ( $T_c$ ) is  
7 measured on recrystallization of the polymer. Higher  $T_c$  values were obtained for hybrid membranes  
8 compared to the pristine membrane. Meanwhile, the melting temperatures can be seen at the broad  
9 endothermic peaks. The peaks at 171.5°C, 172.2°C, and 171.8°C are attributed to melting  
10 temperatures ( $T_m$ ) of the pristine PVDF, 1% MOF/PVDF, and 5% MOF/PVDF membranes,  
11 respectively. The  $T_m$  values are similar for all of the samples. It is known that the  $T_m$  is related with  
12 the lamellae thickness [35]. The stable  $T_m$  values and monotonically higher  $T_c$  show that the AlFu  
13 MOF nucleates the PVDF polymer melt, but doesn't change the crystalline lamellae thickness with  
14 different MOF loadings. Together these trends suggest good polymer-additive compatibility and  
15 dispersion of the AlFu MOF within the PVDF hybrid membranes. Moreover, the degree of  
16 crystallization ( $X_c$ ) for the membranes was also measured and reported in Table 1. 1 % MOF/PVDF  
17 membrane shows a slightly higher crystallinity compared to pristine PVDF membrane, in agreement  
18 with the DSC results discussed above. For the 5% hybrid membrane, there is a decrease in the degree  
19 of crystallinity, suggesting the higher loading of the strongly interacting filler instead disrupts the  
20 efficient packing of the polymer matrix. Fulong et al. [36] also reported that the crystallinity of the  
21 MOF-5/PVDF hybrid membranes decreased with higher MOF loadings. This can be related to the  
22 particle agglomeration phenomenon at high MOF contents, which will reduce the number of the  
23 crystal nucleus as well as the crystallinity.

24 As shown in Fig. 6 (d), the characteristic peaks obtained with the XRD analysis have confirmed  
25 the presence of crystalline nature of MOF, pristine PVDF, and MOF/PVDF membranes. The degree  
26 of crystallinity of the hybrid hollow fiber membranes based on the XRD analysis was also listed in  
27 Table 1, which are in good agreement with the degree of crystallinity from DSC analysis. The  
28 average relative error is only 4.8%. The characteristic peak of MOF at  $2\theta = 31.6$  also appears in the  
29 MOF/PVDF membranes. Moreover, a reduction has been observed in the intensity of the  
30 characteristic peak at  $2\theta = 18.5$  for MOF/PVDF membranes compared to that of the PVDF

1 membrane, while at  $2\theta = 20.1$ , the intensity for MOF/PVDF membranes is a little greater than that  
 2 of the PVDF membrane. This is because the MOF is crystallographic in nature and also displays the  
 3 characteristic peak at around  $2\theta = 20.1$ , leading to the improvement of the intensity for MOF/PVDF  
 4 membranes. The peak associated to PVDF polymer at  $2\theta = 27.3$  decreases significantly with  
 5 inclusion of the 5% MOF dosage, suggesting 5% MOF/PVDF membrane is more amorphous than  
 6 the pure PVDF membrane. This is consistent with the crystallinity results reported in Table 1.

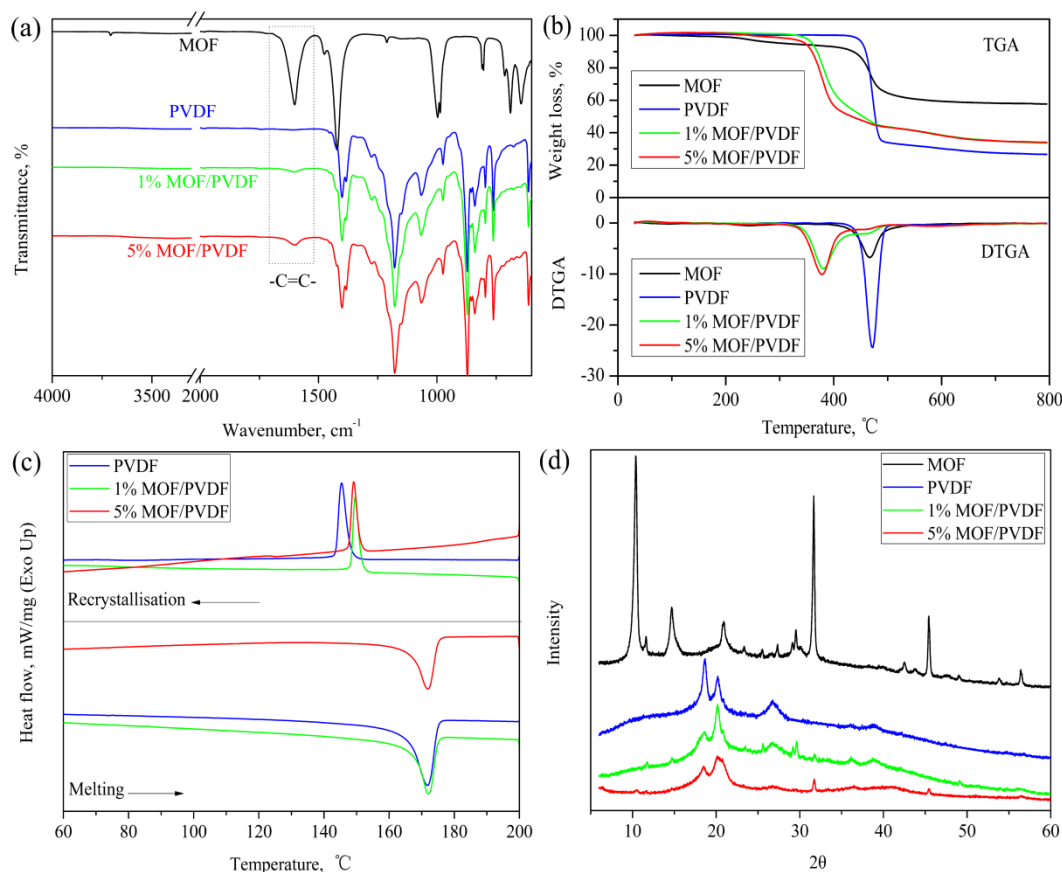


**Fig. 6.** MOF/PVDF hybrid membranes characterizations: (a) FTIR, (b) TGA, (c) DSC, (d) XRD.

**Table 1.**  $T_d$ ,  $T_m$ , and  $T_c$  values and crystallization degree of MOF/PVDF membranes at different MOF dosage.

Sample	$T_d$ , °C	$T_m$ , °C	$T_c$ , °C	$X_c$ , %		
				From DSC	From XRD	Error, %
AlFu MOF	467.8	--	--	--	--	--
PVDF	473.8	171.6	145.4	47.19	42.45	10.0
0.5% MOF/PVDF	406.1	172.2	148.3	47.90	46.09	3.8
1% MOF/PVDF	381.2	172.1	149.6	49.20	47.46	3.5

2% MOF/PVDF	381.1	172.3	149.4	47.49	44.06	7.2
3% MOF/PVDF	373.8	172.0	145.2	41.61	41.31	0.7
4% MOF/PVDF	376.1	172.0	147.6	38.09	36.10	5.2
5% MOF/PVDF	378.7	171.8	149.1	33.66	34.71	3.1

### 3.1.3. Membrane morphology

The prepared MOF/PVDF hybrid hollow fiber membranes' surface and cross-sectional morphology was characterized by scanning electron microscope (SEM). The surface images are shown in Fig. 7 (a1-a7). Changes in inner surface morphology of the PVDF hollow fiber membrane after embedding the MOF particles are clearly evident by the abundance of pores on the membrane surface. The MOF/PVDF hybrid membranes are more porous than the pristine membranes, especially for the MOF dosage of 1%. Higher membrane surface porosity is beneficial for higher permeate flux and thermal efficiency. Sun et al. [37] and Gholami et al. [38] also found that the membrane pore structure of the mixed matrix membrane using hZIF-8 MOF or TMU-5 MOF as fillers could be improved significantly compared to the neat membrane. They believed that the appropriate content of MOF particles may increase the thermodynamic instability and the exchange rate between solvent and non-solvent during the phase inversion process, which finally improved the surface porosity of the prepared hybrid membranes. On the other hand, the nanoparticles could act as extra nucleating agents and penetrate into the polymer lean phase, resulting in the larger pore size and surface porosity of the membrane [17]. However, high MOF loadings cause a larger viscosity of the casting solution, which will induce the kinetic hindrance for solvent exchange in phase inversion [39].

The MOF particles distribution in the MOF/PVDF membranes (Al signal) can be observed from the EDS mapping image (Fig. 7 (a8) and (a9)). As can be seen, MOF particles disperse uniformly in the hybrid MOF/PVDF membranes at low MOF dosages while appear to partially aggregate at MOF dosage of 5%.

Fig. 7 (b1-b3) show the outer surface images of prepared MOF/PVDF hybrid hollow fiber membranes. All the outer surfaces of the pristine PVDF membrane and MOF/PVDF membranes presented similar dense skin-layer as a consequence of the dry phase inversion step of the spinning process (i.e. solvent evaporation along the air gap distance) [40]. It is generally accepted that skin



formation in phase inversion membranes results from a higher local polymer concentration in the outermost region of a nascent membrane compared to the bulk of the dope. This asymmetric distribution of polymer concentration is believed to be caused by solvent evaporation in the air gap and/or multicomponent diffusion in the quench bath [41]. In both these cases, the initially high polymer concentration on the surface of the membrane would produce a lower fraction of polymer-lean phase when phase-separated in the quench bath, leading to a higher density in the skin as compared to the sub-structure.

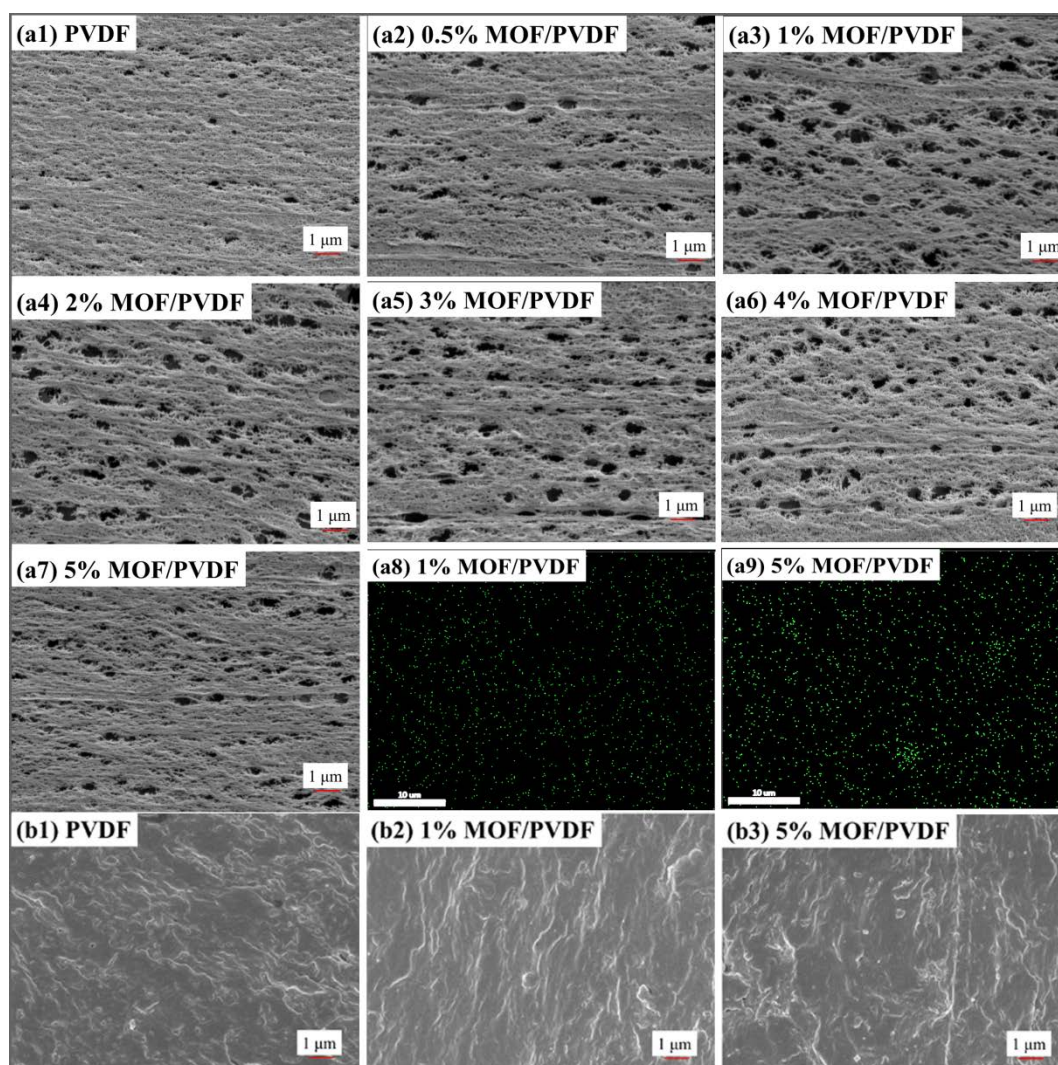


**Fig. 7.** (a1-a7) SEM image of membrane inner surface, (a8-a9) EDS mapping, and (b1-b3) SEM image of membrane outer surface of the prepared MOF/PVDF membrane.

The prepared membranes show similar overall cross-sectional SEM image (shown in Fig. 8 (a1-a3)). The outer diameter and thickness of the membranes is  $1.3 \pm 0.1$  mm and  $195 \pm 5$   $\mu$ m, respectively. The finger-like macrovoids exist on the both sides of PVDF membrane and



MOF/PVDF membrane cross sections and the sponge-like voids locate in the center, displaying a finger-sponge-finger pore structure. With the increasing of MOF dosage, there is an obvious difference for the sponge-like voids of the hybrid membranes. The sponge region of PVDF membrane presents a regular webbed structure (Fig. 8 (a4)). By contrast, a disorganized filamentous structure is shown for 1% MOF/PVDF membrane showing increasing of porosity and enrichment of interconnecting pore passage (Fig. 8 (a5)), whereas adding too much MOF particles leads to a particle agglomeration, as found in the 5% MOF/PVDF membrane (Fig. 8 (a6)). As a result, the 1% MOF/PVDF membrane can produce a larger effective porosity, which will enhance the membrane permeability.

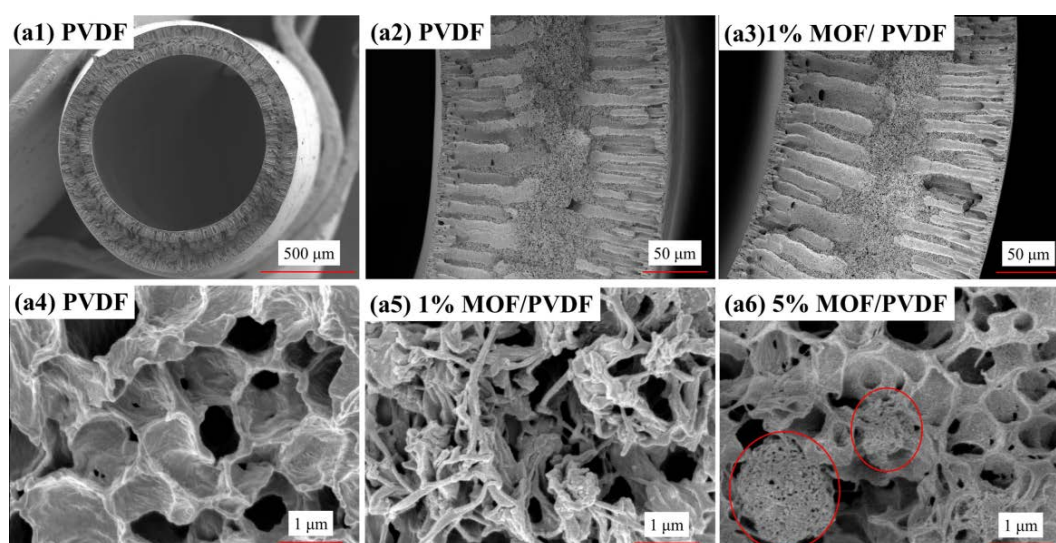


**Fig. 8.** SEM image of membrane cross-section of the prepared MOF/PVDF membranes.

#### 3.1.4. Gas permeation test

Gas permeation flux is a frequently used parameter in evaluation of the stand or fall of permeability of hydrophobic membrane and in determining the pore structure parameters [42]. In general, the higher the gas permeation flux, the higher the MD flux will be. According to Eqs. (S2-S4), the mean pore size and effective porosity of the pristine and hybrid membranes were determined by the gas permeation flux test and the results are shown in Fig. 9 (data listed in Table S3). The membrane porosity can be determined by the combination of the value of the effective porosity and the Eq. (S12) and by the density measurements (e-Component), and the results were also reported in Table S3. The values of the membrane porosity from the density measurement agree well with the ones from gas permeation test, and the average relative error is only 4.4%. This indicates that

1 the membrane porosity from the gas permeation test can be regarded as the membrane bulky  
2 porosity for explaining the performance in DCMD.

3 As can be seen in Fig. 9 (a), compared to the pristine PVDF membrane, the gas permeation  
4 flux of hybrid membranes was considerably improved and shows an initial increasing and then  
5 decreasing trend with the increasing of MOF dosage. The maximum gas permeation flux of the  
6 hybrid membranes is achieved at 1% MOF dosage. The same trend is reflected on the membrane  
7 effective porosity as well as the pore size and porosity as presented in Fig. 9 (b). The highest values  
8 of effective porosity ( $2935 \text{ m}^{-1}$ ) and porosity (0.883) are achieved at the MOF dosage of 1%, which  
9 is consistent with the membrane pore morphology displayed by SEM image (Fig. 7). It is  
10 understandable that the improvement of MOF/PVDF membranes in gas permeation flux is due to  
11 the increased effective porosity of membrane, which is related to the positive effect of MOFs on  
12 facilitating the phase inversion speed and nucleation of polymer in membrane formation [16,37–  
13 39]. However, with the further increase of MOF loading, the observed aggregation of AlFu MOF  
14 particles will lead to the reduction of membrane porosity, and thus resulting in lower gas permeation  
15 flux at high MOF loading.

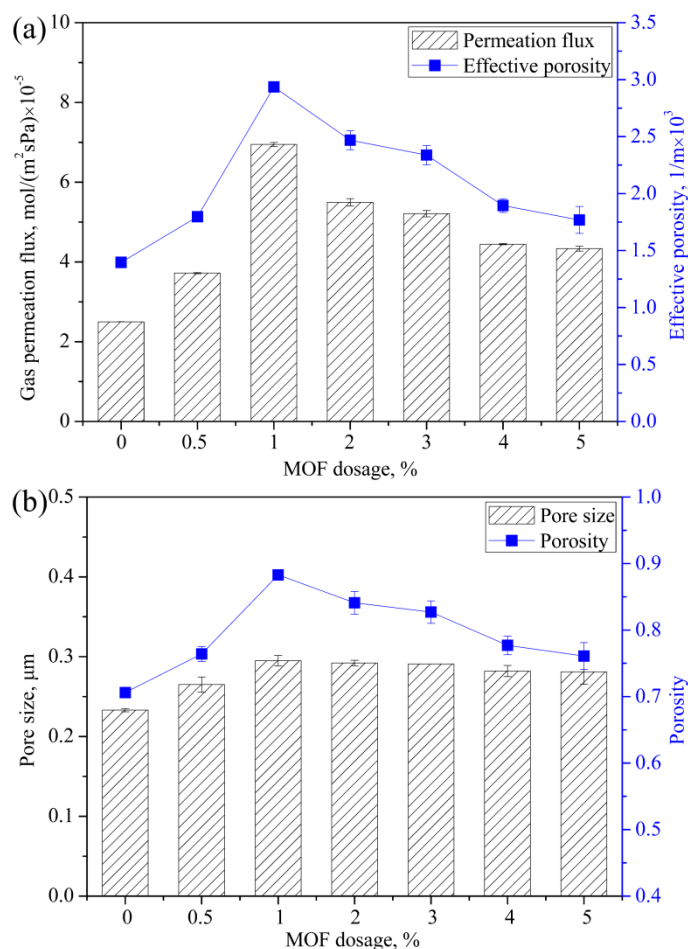


**Fig. 9.** The gas permeation test results of the prepared MOF/PVDF hybrid hollow fiber membranes.

### 3.1.5. Water contact angle (WCA) measurement

The surface hydrophobicity of MD membrane is one of the key parameters affecting membrane selectivity and anti-wetting property. The hydrophobic nature of both the inner and outer hollow fiber membrane surface was evaluated by contact angle measurement and the results are exhibited in Fig. 10. As seen, the incorporation of MOF has little impact on the WCA of the hybrid membranes. The average WCA of the pristine PVDF hollow fiber membrane is  $106^\circ$ . By contrast, the WCA of 5% MOF/PVDF membrane is still higher than  $100^\circ$ . Obviously, the hydrophobic properties of the PVDF membrane are preserved even after MOF addition. The hydrophobicity of the membranes is essential for successful desalination in membrane distillation process.

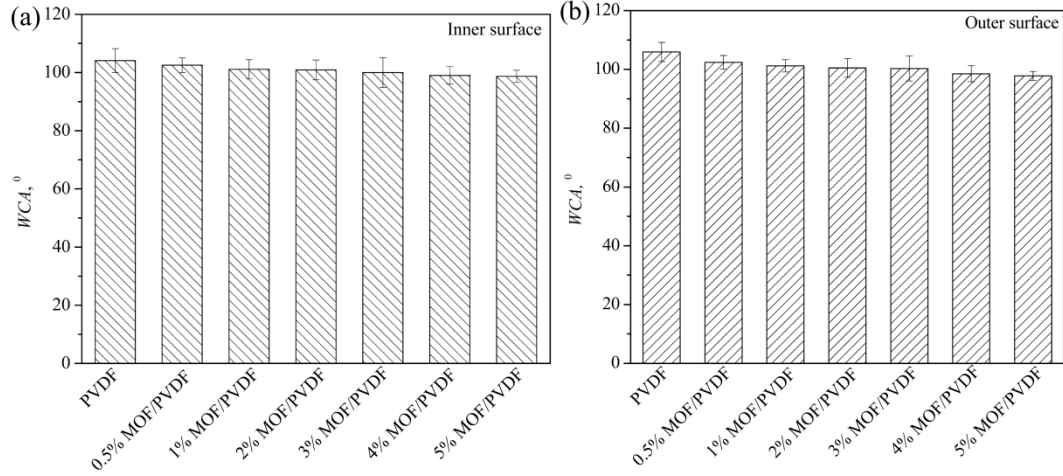


**Fig. 10.** Surface water contact angle of MOF/PVDF hollow fiber membranes.

### 3.2. DCMD performance

#### 3.2.1. Effect of AlFu MOF dosage on permeate flux of membrane

Fig. 10 shows the influence of MOF dosage on the DCMD performance. It can be seen in Fig. 11 (a) that the hybrid membranes achieve higher permeate flux ( $J$ ) than that of pristine PVDF membrane and the  $J$  value reaches to maximum at MOF dosage of 1%. These results are in line with the SEM observation and gas permeation test results which show that the hybrid membranes have higher effective porosity, higher average pore size, and higher gas permeability, especially at MOF dosage of 1%. Meanwhile, the hybrid membranes show as high as 99.9% salt rejection in the MD process which is attributed to the stable water contact angle of the membranes.

The experimental values of  $J$  with different MOF dosages show a good agreement with the predicted  $J$  from the theoretical models described in Section 3. The mean errors are only 7.9% and 9.5% for the feed inlet temperature ( $T_{wf,in}$ ) of 40 °C and 60 °C, respectively, which indicates the validity of the theoretical models. The error is possibly related to the contact of the hollow fibers that will increase channeling and dead zones in the module [43].

According to Eq. (3),  $J$  is mainly dependent on mass transfer coefficient ( $B_T$ ) of membrane under certain operating conditions. The effect of MOF dosages on  $J$  is essentially attributed to its influence on  $B_T$ . The mass transfer coefficients of the hybrid membrane were calculated by the theoretical models and correlated with MOF dosage. As seen in Fig. 11 (b), the  $B_T$  increases with the increase of MOF dosage and reaches to its maximum value at the MOF dosage of 1%. Under the certain operating conditions, the variation of  $B_T$  is associated with the membrane pore structure

parameters according to Eq. (4). Therefore, the effect mechanism of MOF addition on the  $B_T$  of the hybrid membranes is related to the variation of membrane pore structure parameters upon MOF dosage.

The membrane pore structure parameters as well as the heat and mass transfer performance of the hybrid membranes with different MOF loadings were listed in Table 2. As seen, the increasing tendency of mass transfer coefficient and permeate flux is consistent with those of the pore size, porosity, and effective porosity. At 1 wt% MOF dosage, the highest increment in the pore size (16.2%), porosity (25.1%) and effective porosity (52.4%) leads to the most intensive increase of mass transfer coefficient (55.9%) and permeate flux (50.5%). It is interesting to see that the increasing amplitude of mass transfer coefficients is very close to those of effective porosity at all MOF dosages. This is because that according to Eq. (4), under given operating conditions, the  $B_T$  is mainly dependent on the comprehensive effective porosity ( $\varepsilon/(\tau\delta_m)$ ) which integrates the three pore structure parameters of membrane when the pore radii of the membranes are in a narrow range. The relationship is consistent to our previous report that the gas permeation rate and permeate flux of PVDF membranes prepared under different spinning conditions are mainly determined by membrane effective porosity [44].

Furthermore, the remarkable increase of the effective porosity ( $\varepsilon/(\tau\delta_m)$ ) of the hybrid membranes should result from the increase of porosity ( $\varepsilon$ ) and decrease of tortuosity factor ( $\tau$ ) of membrane given stable thickness ( $\delta_m$ ). From Table 2, it is noted that the increment of membrane porosity ( $\varepsilon$ ) is inferior to half of those of the effective porosity ( $\varepsilon/(\tau\delta_m)$ ), which means that the reduction of tortuosity ( $\tau$ ) contribute significantly to the improvement of the effective porosity of the hybrid membranes. Thereby, it can be deduced that the incorporation of MOF in membrane cause a remarkable decrease of the tortuosity of membrane pores, which suggests that the MOF dosage shortens the actual distance travelled by water molecules through the membranes. This is consistent with the observation of membrane pore structure from the cross-sectional SEM image in Figs. 8 (a4) and (a5), from which it can be seen that the sponge-like voids of the hybrid membranes are more porous than the pristine PVDF membrane and the close-knit structure of the PVDF membrane is transformed into a filamentous structure with the MOF dosage. The hybrid membrane pores becomes more inter-connective, which thereby reduces the mass transfer pathways across the membrane. Accordingly, it can be concluded that both the increase in porosity and the simultaneous

reduction in mass transfer route constitute the mechanism of the important role of the MOF on the enhancement of permeability performance of the hybrid membranes in DCMD. In addition, in comparison with hydrophobic PVDF membrane, the MOF particles possess more affinity with water and richer pores larger than water molecules, so it is possible that the dispersion of MOF in the membrane facilitates the capture and fast penetration of water vapor molecules through the membrane.

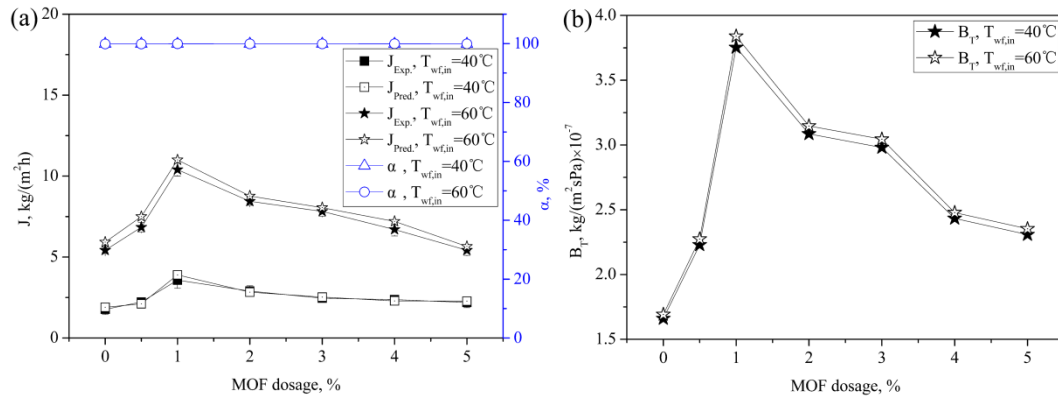


**Fig. 11.** Effect of MOF dosage on (a) permeate flux ( $J$ ) and salt rejection ( $\alpha$ ) and (b) overall mass transfer coefficient ( $B_T$ ).

**Table 2.** The improvement in the pore structural and thermophysical properties and DCMD performance of the hybrid membranes compared to the pristine PVDF membrane ( $T_{wf,in}=40$  °C).

MOF, wt%	$r$ , %	$\varepsilon$ , %	$\varepsilon/(\tau\delta_m)$ , %	$k_{p-m}$ , %	$k_m$ , %	$B_T$ , %	$J$ , %	$\eta$ , %
0.5	6.7	8.2	22.3	-0.2	-12.7	25.6	20.3	24.3
1	16.2	25.1	52.4	-0.4	-38.6	55.9	50.5	46.2
2	15.4	19.1	43.4	-0.7	-29.7	46.2	38.9	38.8
3	15.1	17.1	40.3	-1.1	-26.8	44.4	28.1	35.6
4	12.4	10.0	26.3	-1.5	-16.3	31.7	25.4	27.9
5	12.1	7.8	21.1	-1.8	-12.1	28.1	19.4	23.5

### 3.2.2. Effect of AlFu MOF dosage on thermal efficiency of heat transfer through membrane

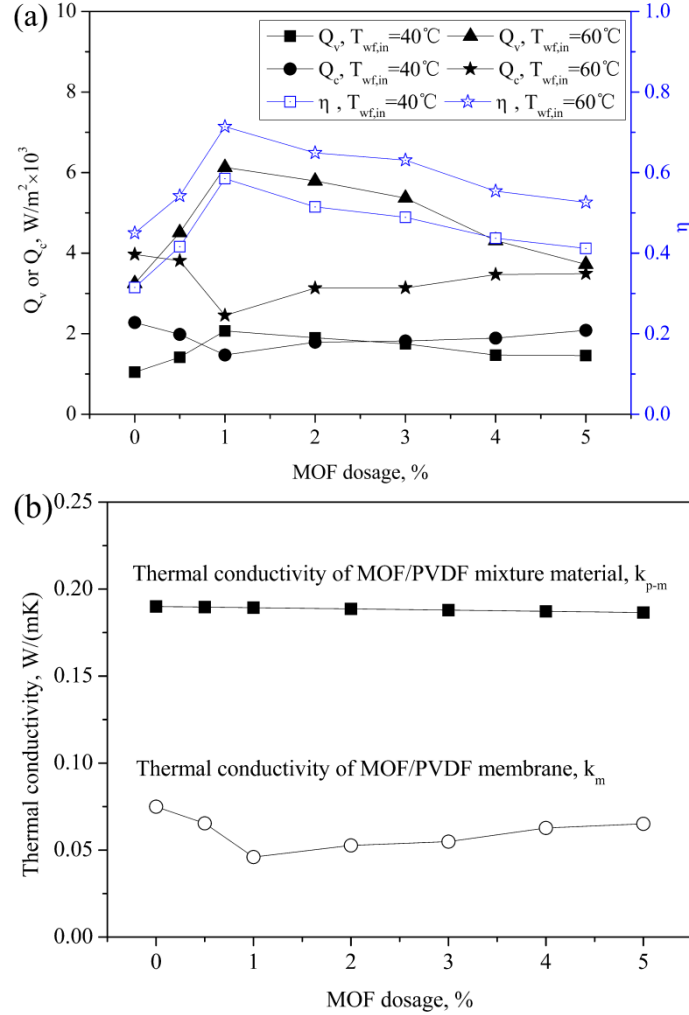
Thermal efficiency of heat transfer through membrane is one of the most important evaluation indexes for MD performance. According to Eq. (8), porous membrane with lower thermal conductivity ( $k_m$ ) offer higher thermal resistances, which will cut down the heat conduction loss

through the membrane ( $Q_c$ ) and in turn increase the thermal efficiency ( $\eta$ ) in DCMD. Fig. 12 (a) shows the effect of MOF dosage on the latent heat of vaporization ( $Q_v$ ), heat transfer through membrane by conduction ( $Q_c$ ), and thermal efficiency ( $\eta$ ). It can be seen that with the variation of MOF dosage, the thermal efficiency increases initially and then decreases, which can be explained by the change of  $Q_v$  and  $Q_c$  with MOF dosage. On the one hand,  $Q_v$  increases by incorporating MOF in membrane (Fig. 12 (a)). This is due to the improved water flux of the hybrid membrane as compared to pristine membrane. As discussed above on Fig. 10, the water flux increases with the increase of MOF dosage and then decreases with the further increase of MOF dosage and the maximum value appears at 1% MOF dosage. Accordingly, the  $Q_v$  shows the same trend as the MOF dosage varies. On the other hand,  $Q_c$  decreases with the increasing of MOF dosage and reaches to its minimum value at 1% MOF dosage and then it increases with the further increase of MOF dosage. Obviously, the MOF dosage in hybrid membranes leads to both the increase in effective heat input and the reduction of heat loss by the thermal conduction, which finally contributes to the improvement of thermal efficiency.

The variation of  $Q_c$  with MOF dosage is related to the membrane thermal conductivity ( $k_m$ ) and temperature difference across the membrane according to Eqs. (S12, S15 and S16). As seen from Eq. (S16), the  $k_m$  is associated with the thermal conductivity of the membrane matrix materials ( $k_{p-m}$ ) and the membrane porosity ( $\varepsilon$ ). As for  $k_{p-m}$  in the hybrid membranes, the thermal conductivity of aluminium fumarate MOF ( $\sim 0.12$  W/(m·K) [33]) is a little bit lower than that of PVDF ( $\sim 0.19$  W/(m·K) [34]), thereof, according to Eq. (S15), the increase of MOF dosage will lead to a reduction in  $k_{p-m}$ . As for  $\varepsilon$ , the air gap in the membrane pores contributes to the reduction of overall membrane thermal conductivity ( $k_m$ ) and the higher the porosity, the lower the  $k_m$  will be. To identify the different contribution of the  $k_{p-m}$  and  $\varepsilon$  to the reduction of  $k_m$ , Fig. 12 (b) compares the  $k_{p-m}$  and  $k_m$  values as function of MOF dosage and the increment percent of  $k_{p-m}$ ,  $k_m$  and  $\eta$  are listed in Table 2. As seen, the  $k_m$  is much lower than  $k_{p-m}$ , and the decrease of  $k_{p-m}$  is only 1.8% with the MOF dosage increasing from 0 to 5 wt% while the reduction of  $k_m$  is as high as 38.6% within the same range of MOF dosage. Therefore, it can be deduced that the much significant reduction of  $k_m$  should be attributed to the high porosity of the hybrid membranes ( $\varepsilon$ ). Thus, it is easy to understand that the 1% MOF/PVDF membrane exhibits the lowest  $k_m$  value because of its highest porosity.

By the above analysis, it can be concluded that the incorporation of MOF increased the porosity

1 of membrane, which leads to the remarkable increase of mass transfer coefficient and also induces  
 2 the significant decrease of thermal conductivity of membrane. This finally results in the  
 3 improvement of permeate flux and thermal efficiency of membrane in DCMD.



4 **Fig. 12.** Effect of MOF dosage on (a) latent heat of vaporization ( $Q_v$ ), heat transfer through membrane by  
 5 conduction ( $Q_c$ ), and thermal efficiency ( $\eta$ ), and (b) thermal conductivity of the MOF/PVDF mixture materials ( $k_{p-}$   
 6  $m$ ) and MOF/PVDF membranes ( $k_m$ ).  
 7

### 8 3.2.3. Stability of membrane performance

9 Considering the higher permeate flux obtained with the 1% MOF/PVDF hollow fiber  
 10 membrane module, long term stability experiment was performed using 1% MOF/PVDF as well as  
 11 pristine PVDF membranes. The operating conditions were feed concentration of 3.5 wt% NaCl,  
 12 feed/permeate inlet temperature of 50°C and 20°C, respectively, and feed/permeate flow rate of 450  
 13 mL/min. The results are presented in Fig. 13. By comparison, the salt rejection for both cases is very



high (> 99.9%) and the 1% MOF/PVDF membrane achieves a higher permeate flux than that of PVDF membrane and shows stable performance. For PVDF pristine membrane, the initial permeate flux is 2.92 kg/(m<sup>2</sup>·h) followed by a continuous decreasing of flux with a reduction of about 27.4% after 50 h running. A partial reason for this decrease of water vapor flux possibly is a partially reversible thermal creep in the membrane with time around the mouth of the partially covered pore [45]. This will increase the mass transfer resistance, and reduce the permeate flux. The 1% MOF/PVDF membrane encounters flux decrease in the first 15 h and then reaches a plateau. The initial flux is 8.04 kg/(m<sup>2</sup>·h) and there is approximately a 15.7% flux reduction after 50 h running, indicating that the MOF/PVDF hybrid hollow fiber membrane module possesses high permeate flux and good operational stability with high salt rejection in DCMD desalination. This also means that the MOF/PVDF hybrid membrane did not suffer any hydrolysis and/or other decomposition mechanism in DCMD process.

Moreover, Table 3 lists a performance comparison between the current work and the previous investigations. As seen, in general, the hybrid membranes exhibited a higher permeate flux compared to the pristine PVDF membrane. It can be also observed that the obtained data in this study is comparable or even better than most of the previous reports. The permeate flux of CaCO<sub>3</sub>/PVDF membrane is higher than that of the MOF/PVDF membrane. But it must be noted that the effective membrane area in ref. [46] was only 0.00502 m<sup>2</sup>, which is nearly one-fifth of the membrane area of this study. Increasing the membrane area under certain operating conditions has a negative effect on the permeate flux [47,48]. It is believed that if the membrane module design optimizations which were attempted in this work are accompanied with reducing membrane area, even higher flux is achievable in DCMD process.

In most studied DCMD processes, the thermal efficiency ranged from 0.1 to 0.7 [9,10,45]. Fan and Peng [49] found that the thermal efficiency of the DCMD process varied from 0.60 to 0.70 when the feed temperature was changed from 50°C to 85°C. In this work, the thermal efficiency of 1% MOF/PVDF hybrid hollow fiber membrane increased from 0.58 to 0.72 when the feed temperature varied from 40°C to 60°C. This means that the thermal efficiency in this work is at a leading level compared to the most reported results for DCMD desalination processes.

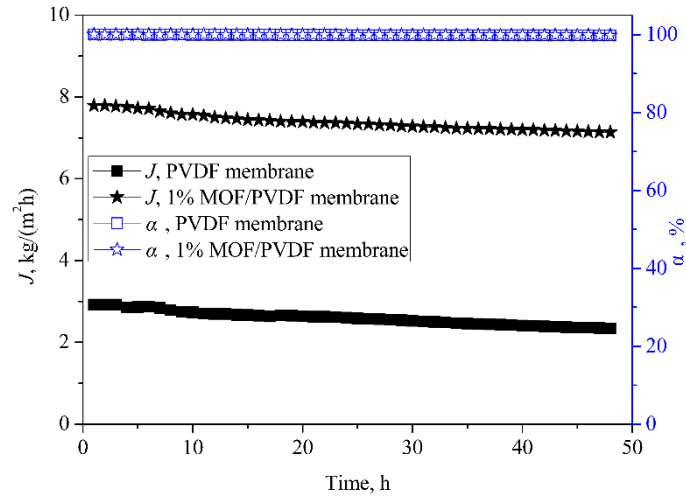


**Fig. 13.** Stability of membrane performance in DCMD desalination of 3.5 wt% NaCl solution.

**Table 3.** performance comparison between the current work and the references for DCMD processes.

Membrane materials	$A/m^2$	Feed side		$T_{wp,in}, ^\circ C$	$J,$ kg/(m <sup>2</sup> ·h)	Ref.
		$T_{wf,in}, ^\circ C$	$C_f$			
PVDF	0.00385	48	3.5 wt%	16	1.83	[15]
MOF/PVDF (PV-5)	0.00385	48	3.5 wt%	16	3.26	[15]
TiO <sub>2</sub> /PVDF	0.00126	40	Pure water	20	~6.5	[50]
PVDF	0.002826	50	Pure water	20	~8.0	[51]
SiO <sub>2</sub> /PVDF	0.002826	50	Pure water	20	~7.5	[51]
PVDF	0.015	80	3.5 wt%	17	5.3	[52]
Clay/PVDF	0.015	80	3.5 wt%	17	5.7	[52]
PVDF	0.00502	50	3.5 wt%	20	~5.1	[46]
CaCO <sub>3</sub> /PVDF	0.00502	50	3.5 wt%	20	~14.0	[46]
PVDF	0.025	50	3.5 wt%	20	2.92	This study
AlFu MOF/PVDF	0.025	50	3.5 wt%	20	8.04	This study
AlFu MOF/PVDF	0.025	70	3.5 wt%	20	15.64	This study

#### 4. Conclusion

In this study, novel MOF/PVDF hybrid hollow fiber membranes were fabricated by incorporating 0.5-5 wt% AlFu MOF into PVDF membrane via phase inversion method. Membrane morphology and gas permeation test results show the increase of membrane pore size (from 0.233  $\mu m$  to 0.297  $\mu m$ ) and porosity upon MOF dosage. With the increasing of MOF dosage, the increment

1 amplitudes of membrane pore size, porosity and effective porosity initially increase and then  
2 decrease. The highest porosity and effective porosity reach 0.88 and 2935 m<sup>-1</sup> at 1% MOF dosage,  
3 respectively, which is higher than pristine PVDF membrane by 25.1% and 52.4%, respectively. The  
4 water flux of hybrid membrane is higher than that of pristine PVDF membrane and shows the same  
5 trend as membrane pore size and porosity with MOF dosage. The mass transfer coefficient of the  
6 MOF/PVDF membrane is primarily dominated by the effective porosity of membrane. At 1% MOF  
7 dosage, the mass transfer coefficient increases by 55.9% due to the same increment of effective  
8 porosity (52.4%). It is found that the increase of effective porosity is attributed to not only the  
9 increase of membrane porosity but also the significant reduction of membrane pore tortuosity. The  
10 appropriate dosage of MOF in membrane shortens the actual distance for water vapor transport  
11 through the membranes by formation of inter-connective pore passage in the hybrid membranes.

12       The MOF dosage in membrane causes the increase in latent heat of vaporization due to the  
13 improved water flux while reduces the thermal conduction loss through the membranes. Both of the  
14 factors lead to the improvement of thermal efficiency in DCMD which reaches to as high as 46.2%  
15 at 1% MOF dosage at a feed temperature of 40°C in treating 1 wt% NaCl aqueous solution. The  
16 reduction of heat conduction across membrane is due to the much significant decline of membrane  
17 thermal conductivity, which results from the remarkable increase of membrane porosity. The  
18 MOF/PVDF membrane shows stable permeability and salt rejection (> 99.9%) for 3.5 wt% NaCl  
19 solution over 50 h DCMD running. This study demonstrates the potential of common porous  
20 materials such as AlFu MOF particles in positive influence of membrane properties toward the  
21 development of high performance membranes for membrane distillation.

## Nomenclature

$J$	Permeate flux, kg/(m <sup>2</sup> ·h)	$\Delta H_v$	Latent heat, kJ/kg
$\alpha$	Salt rejection, %	$J_w$	Gas permeation rate, mol/(m <sup>2</sup> ·s·Pa)
$c$	Salt concentration, wt%	$L_p$	effective pore length, m
$P$	Water vapor pressure, Pa	$\mu$	Viscosity, Pa·s
$\lambda$	Mean free path of molecules, m	$\rho$	Density, kg/m <sup>3</sup>
$k_B$	Boltzmann constant, J/K	$v$	Average velocity, m/s
$\sigma$	Collision diameters of molecules, m	$C_p$	Specific heat, J/(kg·K)
$M$	Molecular weights, g/mol	$Q$	Heat flux, W/m <sup>2</sup>
$B_T$	Mass transfer coefficient, kg/(m <sup>2</sup> ·s·Pa)	$Q_v$	Latent heat by vaporization, W/m <sup>2</sup>
$T$	Temperature, °C	$Q_c$	Heat loss by conduction, W/m <sup>2</sup>
$\delta$	Membrane thickness, m	$\omega$	MOF content, %
$r$	Membrane pore radius, m	$k_{p-m}$	MOF/PVDF thermal conductivity, W/(m·K)
$\varepsilon$	Membrane porosity	$\eta$	Thermal efficiency
$D_w$	Vapor diffusion coefficient, m <sup>2</sup> /s		
$T_{wf,in}$	Feed inlet temperature, °C	<i>Subscripts</i>	
$a_w$	Water activity	$f$	Feed side
$\gamma_w$	Water activity coefficient	$p$	Permeate side
$x_w$	Mole fraction of the solution	$m$	Membrane surface
$h$	Heat transfer coefficient, W/(m <sup>2</sup> ·K)	$b$	Bulk solutions
$k_m$	Thermal conductivity, W/(m·K)	$v$	Vapor
$Nu$	Nusselt number	$w$	Water
$Re$	Reynolds number		
$Pr$	Prandtl number		
$D$	Hydraulic diameter of module, m		

## 1    **Acknowledgments**

2            This work was supported by CSIRO Manufacturing and the National Natural Science  
3    Foundation of China [Grant 21676210]. Dongjian Cheng would like to acknowledge the Ph.D.  
4    mobility scholarship program from Xi'an Jiaotong University. Mr Xiaowei Qian from Xi'an  
5    Jiaotong University is also acknowledged for the assistance of SEM analysis.

## References

- [1] A. Alkhudhiri, N. Darwish, N. Hilal, Membrane distillation: A comprehensive review, *Desalination*. 287 (2012) 2–18. doi:10.1016/j.desal.2011.08.027.
- [2] E. Drioli, A. Ali, F. Macedonio, Membrane distillation: Recent developments and perspectives, *Desalination*. 356 (2015) 56–84. doi:10.1016/j.desal.2014.10.028.
- [3] M.S. El-Bourawi, Z. Ding, R. Ma, M. Khayet, A framework for better understanding membrane distillation separation process, *J. Memb. Sci.* 285 (2006) 4–29. doi:10.1016/j.memsci.2006.08.002.
- [4] P. Wang, T.S. Chung, Recent advances in membrane distillation processes: Membrane development, configuration design and application exploring, *J. Memb. Sci.* 474 (2015) 39–56. doi:10.1016/j.memsci.2014.09.016.
- [5] M. Khayet, Membranes and theoretical modeling of membrane distillation: A review, *Adv. Colloid Interface Sci.* 164 (2011) 56–88. doi:10.1016/j.cis.2010.09.005.
- [6] K.W. Lawson, D.R. Lloyd, Membrane Distillation, *J. Memb. Sci.* 124 (1997) 1–25. doi:10.1016/S0376-7388(96)00236-0.
- [7] N. Thomas, M.O. Mavukkandy, S. Loutatidou, H.A. Arafat, Membrane distillation research & implementation: Lessons from the past five decades, *Sep. Purif. Technol.* 189 (2017) 108–127. doi:10.1016/j.seppur.2017.07.069.
- [8] Y. Peng, Y. Dong, H. Fan, P. Chen, Z. Li, Q. Jiang, Preparation of polysulfone membranes via vapor-induced phase separation and simulation of direct-contact membrane distillation by measuring hydrophobic layer thickness, *Desalination*. 316 (2013) 53–66. doi:10.1016/j.desal.2013.01.021.
- [9] S. Al-Obaidani, E. Curcio, F. Macedonio, G. Di Profio, H. Al-Hinai, E. Drioli, Potential of membrane distillation in seawater desalination: Thermal efficiency, sensitivity study and cost estimation, *J. Memb. Sci.* 323 (2008) 85–98. doi:10.1016/j.memsci.2008.06.006.
- [10] Y. Zhang, Y. Peng, S. Ji, Z. Li, P. Chen, Review of thermal efficiency and heat recycling in membrane distillation processes, *Desalination*. 367 (2015) 223–239. doi:10.1016/j.desal.2015.04.013.
- [11] R. Ullah, M. Khraisheh, R.J. Esteves, J.T. McLeskey, M. AlGhouti, M. Gad-el-Hak, H. Vahedi Tafreshi, Energy efficiency of direct contact membrane distillation, *Desalination*. 433 (2018)

- 1 56–67. doi:10.1016/j.desal.2018.01.025.
- 2 [12] M. Khayet, T. Matsuura, J.I. Mengual, M. Qtaishat, Design of novel direct contact membrane  
3 distillation membranes, *Desalination*. 192 (2006) 105–111. doi:10.1016/j.desal.2005.06.047.
- 4 [13] B.S. Lalia, E. Guillen, H.A. Arafat, R. Hashaikeh, Nanocrystalline cellulose reinforced PVDF-  
5 HFP membranes for membrane distillation application, *Desalination*. 332 (2014) 134–141.  
6 doi:10.1016/j.desal.2013.10.030.
- 7 [14] M. Baghbanzadeh, D. Rana, C.Q. Lan, T. Matsuura, Effects of inorganic nano-additives on  
8 properties and performance of polymeric membranes in water treatment, *Sep. Purif. Rev.* 45  
9 (2016) 141–167. doi:10.1080/15422119.2015.1068806.
- 10 [15] F. Yang, J.E. Efome, D. Rana, T. Matsuura, C. Lan, Metal-organic frameworks supported on  
11 nanofiber for desalination by direct contact membrane distillation, *ACS Appl. Mater.*  
12 *Interfaces*. 10 (2018) 11251–11260. doi:10.1021/acsami.8b01371.
- 13 [16] S. Yang, Q. Zou, T. Wang, L. Zhang, Effects of GO and MOF@GO on the permeation and  
14 antifouling properties of cellulose acetate ultrafiltration membrane, *J. Memb. Sci.* 569 (2019)  
15 48–59. doi:10.1016/j.memsci.2018.09.068.
- 16 [17] M. Baghbanzadeh, D. Rana, C.Q. Lan, T. Matsuura, Effects of hydrophilic silica nanoparticles  
17 and backing material in improving the structure and performance of VMD PVDF membranes,  
18 *Sep. Purif. Technol.* 157 (2016) 60–71. doi:10.1016/j.seppur.2015.11.029.
- 19 [18] I. Erucar, G. Yilmaz, S. Keskin, Recent advances in metal-organic framework-based mixed  
20 matrix membranes, *Chem. - An Asian J.* 8 (2013) 1692–1704. doi:10.1002/asia.201300084.
- 21 [19] R. Lin, B. Villacorta, L. Ge, Z. Zhu, Metal organic framework based mixed matrix membranes:  
22 An overview on filler/polymer interface, *J. Mater. Chem. A*. 6 (2017) 293–312.  
23 doi:10.1039/C7TA07294E.
- 24 [20] S. Kitagawa, R. Kitaura, S.I. Noro, Functional porous coordination polymers, *Angew. Chemie*  
25 *- Int. Ed.* 43 (2004) 2334–2375. doi:10.1002/anie.200300610.
- 26 [21] J. Quirós, K. Boltes, S. Aguado, R.G. de Villoria, J.J. Vilatela, R. Rosal, Antimicrobial metal-  
27 organic frameworks incorporated into electrospun fibers, *Chem. Eng. J.* 262 (2015) 189–197.  
28 doi:10.1016/j.cej.2014.09.104.
- 29 [22] X. Li, Y. Liu, J. Wang, J. Gascon, J. Li, B. Van Der Bruggen, Metal-organic frameworks based  
30 membranes for liquid separation, *Chem. Soc. Rev.* 46 (2017) 7124–7144.

doi:10.1039/C7CS00575J.

[23] J. Jiang, Molecular simulations in metal-organic frameworks for diverse potential applications, *Mol. Simul.* 40 (2014) 516–536. doi:10.1080/08927022.2013.832247.

[24] N.U. Qadir, S.A.M. Said, H.M. Bahaidarah, Structural stability of metal organic frameworks in aqueous media - Controlling factors and methods to improve hydrostability and hydrothermal cyclic stability, *Microporous Mesoporous Mater.* 201 (2015) 61–90. doi:10.1016/j.micromeso.2014.09.034.

[25] J. Zuo, T.S. Chung, Metal-organic framework-functionalized alumina membranes for vacuum membrane distillation, *Water (Switzerland)*. 8 (2016) 1–15. doi:10.3390/w8120586.

[26] E. Alvarez, N. Guillou, C. Martineau, B. Bueken, B. Vandevorde, C. Leguillouzer, P. Fabry, F. Nouar, F. Taulelle, D. Devos, J.S. Chang, K.H. Cho, N. Ramsahye, T. Devic, M. Daturi, G. Maurin, C. Serre, The structure of the aluminum fumarate metal-organic framework A520, *Angew. Chemie - Int. Ed.* 54 (2015) 3664–3668. doi:10.1002/anie.201410459.

[27] S. Karmakar, S. Bhattacharjee, S. De, Aluminium fumarate metal organic framework incorporated polyacrylonitrile hollow fiber membranes: Spinning, characterization and application in fluoride removal from groundwater, *Chem. Eng. J.* 334 (2018) 41–53. doi:10.1016/j.cej.2017.10.021.

[28] S. karmakar, J. Dechnik, C. Janiak, S. De, Aluminium fumarate metal-organic framework: A super adsorbent for fluoride from water, *J. Hazard. Mater.* 303 (2016) 10–20. doi:10.1016/j.jhazmat.2015.10.030.

[29] M. Rubio-Martinez, T.D. Hadley, M.P. Batten, K. Constanti-Carey, T. Barton, D. Marley, A. Mönch, K.S. Lim, M.R. Hill, Scalability of continuous flow production of metal-organic frameworks, *ChemSusChem*. 9 (2016) 938–941. doi:10.1002/cssc.201501684.

[30] M. Rubio-Martinez, C. Avci-Camur, A.W. Thornton, I. Imaz, D. Maspoch, M.R. Hill, New synthetic routes towards MOF production at scale, *Chem. Soc. Rev.* 46 (2017) 3453–3480. doi:10.1039/c7cs00109f.

[31] K. Li, J.F. Kong, D. Wang, W.K. Teo, Tailor-made asymmetric PVDF hollow fibers for soluble gas removal, *AIChE J.* 45 (1999) 1211–1219. doi:10.1002/aic.690450607.

[32] D. Wang, K. Li, W.K. Teo, Preparation and characterization of polyvinylidene fluoride (PVDF) hollow fiber membranes, *J. Memb. Sci.* 163 (1999) 211–220. doi:10.1016/S0376-



- 1 7388(99)00181-7.
- 2 [33] F. Jeremias, D. Fröhlich, C. Janiak, S.K. Henninger, Advancement of sorption-based heat  
3 transformation by a metal coating of highly-stable, hydrophilic aluminium fumarate MOF,  
4 RSC Adv. 4 (2014) 24073–24082. doi:10.1039/c4ra03794d.
- 5 [34] I. Hitsov, T. Maere, K. De Sitter, C. Dotremont, I. Nopens, Modelling approaches in membrane  
6 distillation: A critical review, Sep. Purif. Technol. 142 (2015) 48–64.  
7 doi:10.1016/j.seppur.2014.12.026.
- 8 [35] S. Lanceros-Mendez, J.F. Mano, A.M. Costa, V.H. Schmidt, FTIR and DSC studies of  
9 mechanically deformed  $\beta$ -PVDF films, J. Macromol. Sci. Part B. 40 (2001) 517–527.  
10 <http://www.tandfonline.com/doi/abs/10.1081/MB-100106174>.
- 11 [36] C.R.P. Fulong, J. Liu, V.J. Pastore, H. Lin, T.R. Cook, Mixed-matrix materials using metal-  
12 organic polyhedra with enhanced compatibility for membrane gas separation, Dalt. Trans. 47  
13 (2018) 7905–7915. doi:10.1039/c8dt00082d.
- 14 [37] H. Sun, B. Tang, P. Wu, Hydrophilic hollow zeolitic imidazolate framework-8 modified  
15 ultrafiltration membranes with significantly enhanced water separation properties, J. Memb.  
16 Sci. 551 (2018) 283–293. doi:10.1016/j.memsci.2018.01.053.
- 17 [38] F. Gholami, S. Zinadini, A.A. Zinatizadeh, A.R. Abbasi, TMU-5 metal-organic frameworks  
18 (MOFs) as a novel nanofiller for flux increment and fouling mitigation in PES ultrafiltration  
19 membrane, Sep. Purif. Technol. 194 (2018) 272–280. doi:10.1016/j.seppur.2017.11.054.
- 20 [39] A. Zirehpour, A. Rahimpour, S. Khoshhal, M.D. Firouzjaei, A.A. Ghoreyshi, The impact of  
21 MOF feasibility to improve the desalination performance and antifouling properties of FO  
22 membranes, RSC Adv. 6 (2016) 70174–70185. doi:10.1039/c6ra14591d.
- 23 [40] L. García-fernández, M.C. García-payo, M. Khayet, Mechanism of formation of hollow fiber  
24 membranes for membrane distillation : 1 . Inner coagulation power effect on morphological  
25 characteristics, J. Memb. Sci. 542 (2017) 456–468. doi:10.1016/j.memsci.2017.03.036.
- 26 [41] D.T. Clausi, W.J. Koros, Formation of defect-free polyimide hollow fiber membranes for gas  
27 separations, J. Memb. Sci. 167 (2000) 79–89.
- 28 [42] L. Zhao, X. Lu, C. Wu, Q. Zhang, Flux enhancement in membrane distillation by incorporating  
29 AC particles into PVDF polymer matrix, J. Memb. Sci. 500 (2016) 46–54.  
30 doi:10.1016/j.memsci.2015.11.010.

- 1 [43] F. Lipnizki, R.W. Field, Mass transfer performance for hollow fibre modules with shell-side  
2 axial feed flow: using an engineering approach to develop a framework, *J. Memb. Sci.* 193  
3 (2001) 195–208. doi:10.1016/S0376-7388(01)00512-9.
- 4 [44] Y. Tang, N. Li, A. Liu, S. Ding, C. Yi, H. Liu, Effect of spinning conditions on the structure  
5 and performance of hydrophobic PVDF hollow fiber membranes for membrane distillation,  
6 *Desalination*. 287 (2012) 326–339. doi:10.1016/j.desal.2011.11.045.
- 7 [45] B. Li, K.K. Sirkar, Novel Membrane and Device for Direct Contact Membrane Distillation-  
8 Based Desalination Process, *Ind. Eng. Chem. Res.* 43 (2004) 5300–5309.  
9 doi:10.1021/ie030871s.
- 10 [46] Y. Song, Z. Wang, Q. Wang, B. Li, B. Zhong, Preparation of PVDF/CaCO<sub>3</sub> hybrid hollow  
11 fiber membranes for direct contact membrane distillation through TIPS method, *J. Appl.*  
12 *Polym. Sci.* (2016) 43372. doi:10.1002/app.43372.
- 13 [47] D. Cheng, W. Gong, N. Li, Response surface modeling and optimization of direct contact  
14 membrane distillation for water desalination, *Desalination*. 394 (2016) 108–122.  
15 doi:10.1016/j.desal.2016.04.029.
- 16 [48] G. Guan, X. Yang, R. Wang, A.G. Fane, Evaluation of heat utilization in membrane distillation  
17 desalination system integrated with heat recovery, *Desalination*. 366 (2015) 80–93.  
18 doi:10.1016/j.desal.2015.01.013.
- 19 [49] H. Fan, Y. Peng, Application of PVDF membranes in desalination and comparison of the VMD  
20 and DCMD processes, *Chem. Eng. Sci.* 79 (2012) 94–102. doi:10.1016/j.ces.2012.05.052.
- 21 [50] N. Hamzah, C.P. Leo, Membrane distillation of saline with phenolic compound using  
22 superhydrophobic PVDF membrane incorporated with TiO<sub>2</sub> nanoparticles: Separation, fouling  
23 and self-cleaning evaluation, *Desalination*. 418 (2017) 79–88. doi:10.1016/j.desal.2017.05.029.
- 24 [51] J. Zhang, Z. Song, B. Li, Q. Wang, S. Wang, Fabrication and characterization of  
25 superhydrophobic poly (vinylidene fluoride) membrane for direct contact membrane  
26 distillation, *Desalination*. 324 (2013) 1–9. doi:10.1016/j.desal.2013.05.018.
- 27 [52] J.A. Prince, G. Singh, D. Rana, T. Matsuura, V. Anbharasi, T.S. Shanmugasundaram,  
28 Preparation and characterization of highly hydrophobic poly(vinylidene fluoride) - Clay  
29 nanocomposite nanofiber membranes (PVDF-clay NNMs) for desalination using direct contact  
30 membrane distillation, *J. Memb. Sci.* 397–398 (2012) 80–86.

- 1        doi:10.1016/j.memsci.2012.01.012.
- 2